Invited Paper

A 2D quadrangular pyramid photoelectric autocollimator with extended angle measurement range*

Konyakhin Igor[1], LI Renpu (黎人溥)[2], ZHOU Min (周敏)[3], Dang Dinh Duan[1], Nikitin Mikhail[1], HUANG Guifu (黄贵伏)[2], YANG Jiawen (杨嘉文)[2], and TAN Xin (谭鑫)[2]**

1. Faculty of Applied Optic, ITMO University, 49 Kronverkskiy Prospect, Saint Petersburg 197101, Russia

2. Chongqing Engineering Research Center of Intelligent Sensing Technology and Microsystem, Chongqing University of Post and Telecommunications, Chongqing 400065, China

3. School of Communication and Information Engineering, Chongqing University of Posts and Telecommunications, Chongqing 400065, China

(Received 9 September 2020; Revised 4 January 2021)

A photoelectric autocollimator with high accuracy and extended measurement range based on the quadrangular pyramid is proposed, and the corresponding algorithms are also deduced. A new image processing algorithm has been proposed to improve the accuracy, and the corresponding errors are also estimated, the error does not exceed half a pixel when the distance between the marks more than two radii. The experimental results have verified that the measurement range of the proposed two-dimensional (2D) quadrangular pyramid photoelectric autocollimator can be increased $\sqrt{2}$ times than that of the flat mirror photoelectric autocollimator from 10′ to 15′. The accuracy is better than 1″ when the deflection is less than 15′.

Document code: A **Article ID:** 1673-1905(2021)08-0468-7

DOI https://doi.org/10.1007/s11801-021-0141-3

Angle measurement is widely used in enterprises of mechanical engineering and the optical industry to measure the deviations from the straightness guide, deviation from planarity faceplate and surface plate, configuration tools and machines, the analysis of vibration and temperature changes, as well as measuring the angles of optical wedges. Optoelectronic systems allow non-contact, quickly and with high precision solve the given tasks[1-3]. The photoelectric autocollimator is an important measuring instrument for small-angle measurement based on the principal of optical autocollimating, which is widely used in the fields of industrial production, national defense technology and scientific research[4-7]. However, the small measurement range of the autocollimators greatly restricts the applications and developments of autocollimators in the field of industrial measurement.

For the large measurement range requirement of the autocollimator, the methods to expand the measurement range has gradually become the research focus in recent years[8-14]. To extending the measurement range of the autocollimator, the authors have proposed a type of laser autocollimator by utilizing a multi-cell photodiode (PD) array, and the measurement range of the laser autocollimator has been improved to be larger than 2 000″[10]. However, a specified cell width and an extremely small cell gap are needed for the PD array, which cannot be satisfied by a commercially available product. In 2014, K Ishikawa et al[11] proposed a new method of measuring large aspherical optical surfaces using a rotating accuracy autocollimator, and the measuring range is 4 500″. A 6*N*+2 dimension optimization (where *N* is the number of scan lines taken across the mirror) was proposed to extend the angular measurement range of the autocollimator[12]. However, this system is susceptible to the effects of the numerical noise, which would decrease the measuring accuracy. In 2016, Chen et al[13] has developed a laser autocollimator with a measurement range of 11 000″ by utilizing a mode-locked laser and a diffraction grating as the light source and the reflector, respectively. In the second year, with the optical frequency domain angle measurement method, the measurement range has been increased to 21 600″[14], which is a significant extension from a conventional laser autocollimator. Nevertheless, due to the limitation of beam expansion and

* This work has been supported by the National Key R&D Program of China (No.2020YFC2003301), the National Natural Science Foundation of China (Nos.62005033, 61705027, 11704053, 51902037 and 61901069), the Government of the Russian Federation (No.08-08), the Basic Research Project of Chongqing Science and Technology Commission (No.CSTC-2020jcyj-msxm0603), and the Science and Technology Research Program of Chongqing Municipal Education Commission (No.KJQN202000609).

** E-mail: minzhou2020@163.com

the caliber for lens, the system cannot be used to measure a larger tilt angle, and the complex structure of this system would increase the cost.

In this paper, a large dynamic range, high precision two-dimensional (2D) photoelectric autocollimator based on quadrangular pyramid is proposed and demonstrated, and the algorithms of which are also deduced. For further increasing the accuracy, a new image processing algorithm has been proposed, and the corresponding errors are also estimated. The research demonstrates that the error is less than a pixel, and the error does not exceed half a pixel when the distance between the marks more than two radii. Also, worth noting is the possibility of the algorithm to work with any number of marks and high noise immunity. The angle measurement experiments have been carried out to demonstrate the feasibility of the proposed method, and the experimental results have verified that the measurement range of the proposed quadrangular pyramid photoelectric autocollimator can be increased $\sqrt{2}$ times than that of the flat mirror photoelectric autocollimator, the accuracy is better than 1″ when the deflection is less than 20′.

The traditional 2D optical-electronic autocollimation system includes autocollimator mounted on the fixed, and a flat mirror is used as a reflector placed on inspected object, which is shown in Fig.1. Autocollimator consists of emitting optic-electronics channel and a receiver with a microprocessor. Emitting channel generates an optical beam that falls on the reflector. Optical electronic receiver meant for registration of optical radiation from the control element and measuring its parameters, which determine rotation angles of the object. When turning mirrors on the angles Θ_1 as tilt and Θ_2 as yaw relative to the collimation axes, the reflected beam is coming back in the autocollimator lens with deflection to the full angle $2\sqrt{\Theta_1^2+\Theta_2^2}$ from the optical axis of the lens. As a result, the image shifts on the matrix photo-receiver of the autocollimator. The microprocessor calculates video frames from the matrix photo-receiver and determines the shift of the image. However, the measurement range of the autocollimator cannot be expanded significantly with a flat mirror. One of the reasons is significant displacement of the reflected beam in the plane of the aperture of the lens in the presence of both angles of rotation relative to the two collimation axes.

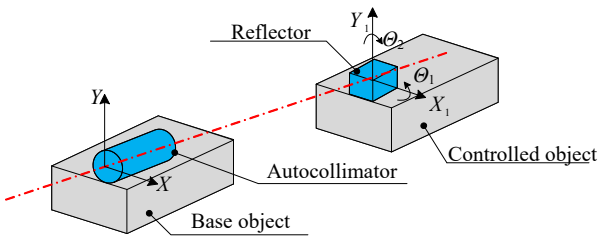

Fig.1 The structure of the traditional autocollimator

In this paper, a glass quadrangular pyramid is proposed to replace the flat mirror as the reflector of the autocollimator to expand the measurement range, which is shown in Fig.2(a). Each pair of opposite faces of the quadrangular pyramid is equivalent to the right-angle prism Porro[15]. Therefore, the parallel beam incident on the refractive face at the reflection, is divided into two beams, each of which is formed a corresponding equivalent right-angle prism Porro. By rotating the pyramid relative to one axis on tilt Θ_1 or yaw Θ_2, each reflected beam will move only along this axis in the plane of the aperture of the objective while the other coordinates of its position will not change. As a result, at the two-coordinate measuring the angle of deflection of the working beam from the optical axis is also equal to $2\Theta_1$ (or $2\Theta_2$).

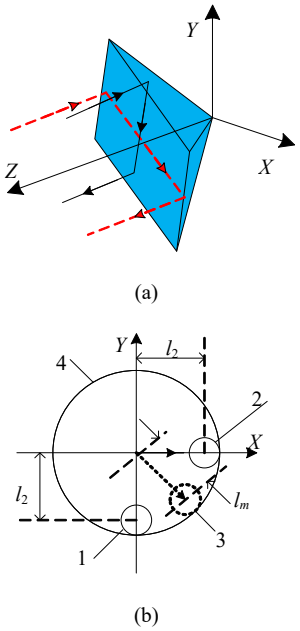

Fig.2 (a) The quadrangular pyramidal reflector; (b) The spots on the plane of the aperture of objective, where 1,2 are the pyramidal reflectors, 3 is the mirror reflector, and 4 is the aperture of objective

By rotating the conventional mirror reflector on tilt Θ_1 and yaw Θ_2, the reflected beam moves along two axes. As a result, at the two-coordinate measuring the angle of deflection of the working beam from the optical axis is equal to $2\sqrt{\Theta_1^2+\Theta_2^2}$.

The valid shifts l_1, l_2, l_m of the reflected beam spots in the plane of the aperture the objective for small angles of rotation can be calculated by

$$l_1=2\Theta_1\cdot L,\quad l_m=2\sqrt{\Theta_1^2+\Theta_2^2}\cdot L, \tag{1}$$

where L is the distance to reflector.

Therefore, the required diameter of the lens for receiving both of these beams is $\sqrt{2}$ times smaller, than that for the flat mirror reflected beam (with equal measurement ranges of angles Θ_1 and Θ_2), as shown in

Fig.2(b). This allows us to increase $\sqrt{2}$ times the measurement range of the 2D autocollimator by simple replacement of the reflecting control element and use of software to implement the requisite image processing algorithm.

Unit vector $\boldsymbol{B}$ of the reflected beam after the reflector has been moved is calculated by[16]

$$\boldsymbol{B}=\boldsymbol{M}_r\cdot\boldsymbol{M}_d\cdot\boldsymbol{M}_r^{-1}\boldsymbol{A}, \tag{2}$$

where $\boldsymbol{A}$ is the unit vector of the beam incident on the reflector, $\boldsymbol{M}_d$ is reflection matrix associated with the reflector in the coordinate system $X_1Y_1Z_1$[17], $\boldsymbol{M}_r$ and $\boldsymbol{M}_r^{-1}$ are matrices of forward and reverse operators determining the direct and inverse transitions between the XYZ coordinate systems and $X_1Y_1Z_1$. Form of the matrix $\boldsymbol{M}_r$ is defined by the formula from Ref.[18] under replacing $\Theta_1=\nu$, $\Theta_2=\psi$, $\Theta_3=0$.

The action of the selected reflector is equivalent to the action of the two right-angle prisms with the mutually perpendicular edges of the dihedral angles between the reflecting faces.

For right-angle prism with the unit vector of edge $\overline{\boldsymbol{P}}_1=\begin{bmatrix}0\\1\\0\end{bmatrix}$ matrix of action is determined by substituting the coordinates of the unit vector of the general form[19]:

$$\boldsymbol{M}_{d1}=\begin{bmatrix}-1&0&0\\0&1&0\\0&0&-1\end{bmatrix}. \tag{3}$$

For right-angle prism with the unit vector $\overline{\boldsymbol{P}}_2=\begin{bmatrix}1\\0\\0\end{bmatrix}$, the matrix is equal:

$$\boldsymbol{M}_{d2}=\begin{bmatrix}1&0&0\\0&-1&0\\0&0&-1\end{bmatrix}. \tag{4}$$

When turning the object, with which is associated a reflector, on the angles Θ_1, Θ_2, the coordinates of the unit vectors $\boldsymbol{B}_{1,2}$ of two reflected beams along the axes OX, OY are determined from expressions:

$$\boldsymbol{B}_{x1}=0,\ \boldsymbol{B}_{y1}=-\sin(2\Theta_1), \tag{5}$$

$$\boldsymbol{B}_{x2}=\sin(2\Theta_2)\cdot\cos(\Theta_1),\ \boldsymbol{B}_{y2}=\sin(2\Theta_1)\cdot\sin^2(\Theta_2). \tag{6}$$

Here the number in the index identifies the number of the reflected beam, the upper line and the sign in the structure part of formulas corresponds to the unit vector of the first beam.

Two reflected beams are formed in the photodetector plane of the receiving channels of the marked autocollimator images 1 and 2. These images are shifted at the values y_1 and x_2, y_2 on the axes OX and OY (Fig.3):

$$y_1=f\cdot\mathrm{tg}\beta_1,\ x_2=f\cdot\mathrm{tg}\alpha_2,\ y_2=f\cdot\mathrm{tg}\beta_2, \tag{7}$$

where f is the focal length of the autocollimator lens, β_1, α_2 and β_2 are the angles between the projections of the unit vectors $\boldsymbol{B}_{1,2}$ in the coordinate planes YOZ, XOZ and the optical axis of the lens, respectively.

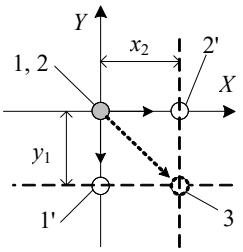

Fig.3 The image on the photodetector matrix, 1, 2: before the rotation of the reflector; 1′, 2′: after the rotation; 3: hypothetic position for the mirror reflector

The angles α and β are actually longitude and latitude of the unit vector of the reflected beam in a polar coordinate system (the OZ axis parallel to the optical axis is a polar axis). The coordinates of the unit vectors of the reflected beams in the XYZ coordinate system associated with the longitude and latitude through the known relations:

$$\boldsymbol{B}_{y1}=\sin\beta_1,\ \boldsymbol{B}_{x2}=\sin\alpha_2\cdot\cos\beta_2,\ \boldsymbol{B}_{y2}=\sin\beta_2. \tag{8}$$

Eqs.(5)—(8) define a system of three nonlinear equations formed through equating of their right sides. This system comprises equations corresponding to the unit vectors of the two beams.

Use of this algorithm requires a microprocessor to be included in the autocollimator unit. For small measured angles, an approximate algorithm can be used as follows:

$$\boldsymbol{B}_{y1}=\beta_1=-2\Theta_1,\ \boldsymbol{B}_{x2}=\alpha_2=2\Theta_2, \tag{9}$$

$$\Theta_1=-y_1/(2f),\ \Theta_2=x_2/(2f). \tag{10}$$

In this case, the image-processing algorithm can be implemented with a simple electronic processing unit based on logical microcircuits of medium-scale integration level.

The foremost stage of the calculation of the angles Θ_1 and Θ_2 is to determine the center of the marks registered by the system. Using the control elements different from flat mirror creates a situation when in the image plane will mark overlap with each other. In this connection, the question arises what should be the distance between the centers of the marks in order to save serviceability and accuracy of the measurement system.

To study the possible solution of this problem has been developed and implemented a model for the processing of overlapping arrays of irradiance in technology MatLab, and the model parameters are shown in Tab.1. This model has allowed to investigate the influence marks overlapping on the measuring accuracy of the coordinates.

In general, the idea of the algorithm consists in preliminary find the most probable centers of marks and their subsequent a clarification by the weighted summation method. To minimize the effect marks overlapping decided to use one of the key features of the control element,

namely the fact that each mark can move only along one axis.

Tab.1 The model parameters

Parameter	Value
The size of the matrix	128 pixel×128 pixel
The radius of the mark	12 pixels
Signal-to-noise ratio	17
The law of distribution of noise	Normal

The previous stage of the algorithm is to prepare the image to be processed. At this action, the image processing by the circular averaging filter with a window size equal to the diameter of a circle plus one pixel. Then apply a threshold filtering that allows to cut noise. After filtering threshold is necessary to apply a Gaussian filter as the image becomes unusable for processing by a weighted summation method[20,21].

To solve the overlapping problem, a priori known information about the geometric form of the mark is used. In this system, the mark has a circular shape, which makes it stable to noise and invariant to rotation, scale, etc. A circle can be described by an equation with three parameters (x, y, R), where r is the radius of the circle. Thus, the primary task is to detect geometric primitives corresponding to a given combination of parameters.

For these purposes, it developed an algorithm based on the Hough transform[20,21]. It allowed a high speed and accurately determine the coordinates of the marks, to measure them, and maintain the mark in the course of their movement, even in the case of their intersection. It should be noted that in the case of a complete intersection, when more than 60% of the surfaces coincide, the support becomes impossible. However, now our team is working to improve the algorithm in order to solve this problem.

Hough transform is perfect for this since it is able to work with geometric primitives, noise immunity, and the equation of a circle.

$$(x^2+y^2)=R^2. \tag{11}$$

Allows determining the coordinates of the center i.e. x and y after detection. Using the equation of a circle in Cartesian coordinates will create a three-dimensional space of the accumulation, in which calculations will be performed. Thus, in the first stage of the algorithm the simulated frame is transformed to grayscale view, as shown in Fig.4.

This is necessary for the correct operation of the algorithm. When conversion was done, the algorithm needs to know the range of possible values for the radius of the mark, as well as the value of the threshold filter for further processing. These values can be pre-recorded in the algorithm when configured for each new situation. To study the algorithm, these parameters were selected once and used consistently in all experiments.

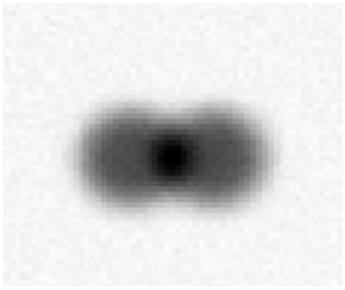

Fig.4 Simulation results after the grayscale image transformation (the colors are inverted)

In the second stage, the algorithm calculates the gradient value in each direction and then calculates the gradient magnitude from formula:

$$\nabla img = \sqrt{(\nabla img_x)^2 + (\nabla img_y)^2}\ , \tag{12}$$

where ∇img is gradient magnitude, ∇img_x and ∇img_y are gradient horizontally and vertically, respectively.

The points that will be used for voting, for the subsequent determination of the center of the circle are detected in the received array. For this purpose, the value is compared with the threshold value (specified together with the range of radii). The pixel background is excluded from the voice due to this. The result of the step is shown by Fig.5.

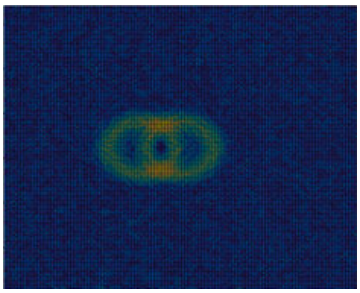

Fig.5 The result of estimating the value of the gradient vector (the colors are inverted)

At the third stage, the accumulation array is formed. The dimension of this array always coincides with the number of variables that define the geometric primitive. Already at this stage, it is possible to select the boundaries of marks. Fig.6 shows the accumulation array, where the horizontal and vertical axes represent the pixel coordinates of the photodetector, and the unit is arbitrary.

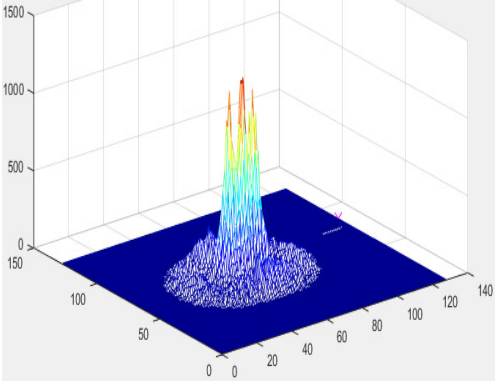

Fig.6 3D view of accumulation array

For the coordinates of the mark centers calculations, it is necessary to calculate the local maxima in the space of the accumulation array (Stage 4).

For this purpose, the array is divided into parts. The minimum part size can be one-quarter of the short side of the matrix or 1.5 the maximum possible radius of the mark. Between these values, the minimum is chosen and is assigned as the size of the "area of interest".

After the zones of interest were selected, each of them is analyzed for the presence of identical near-standing pixels (not less than 8) with a value above the specified level. Each such group of pixels is assigned its own index. For each such group, there is a local maximum. Fig.7 shows the filtered accumulation array, where the horizontal and vertical axes represent the pixel coordinates of the photodetector, and the unit is arbitrary.

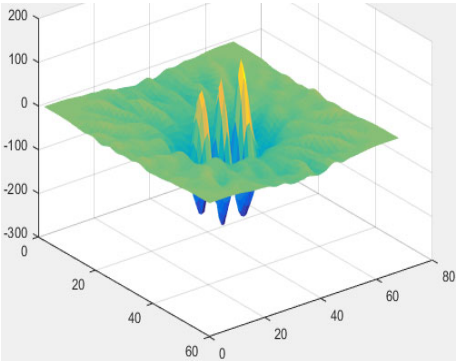

Fig.7 Accumulation array after local maximum filtering

Among the candidates that have been formed, group by contiguity was formed, and the center of gravity for each group is calculated. Obviously, the middle positioned maximum is the result of the adding of the overlapped intensities. In this case it isn't analyzed in Final stage. Two another centers will be the centers of the circles i.e. marks images. These coordinates are superimposed on the original image and display the detected circles and their centers in the output simulated frame. The result of the program is shown in Fig.8, which is to display the result in the image plane with an indication of the measured centers of coordinates and the distance between the centers.

These stages were made by using Digital Image Processing Toolbox in Matlab[22].

In the process of algorithm research, the model was used to evaluate the error, and a two-step simulation was carried out:

Step 1: The distance between the image centers is set as L, changing the step size from $0.5R$ to $1.9R$ with a step length of $0.1R$ (where R is the radius of the marked image). In this process, the phenomenon of overlapping marks imagines is involved. To ensure the accuracy of the image center coordinates, a processing algorithm based on the Hough transform is adopted, which has been discussed above). Comparing the measured image coordinates (x, y) with the original accurate values, and the simulation result is shown in Fig.9 (the black and red lines).

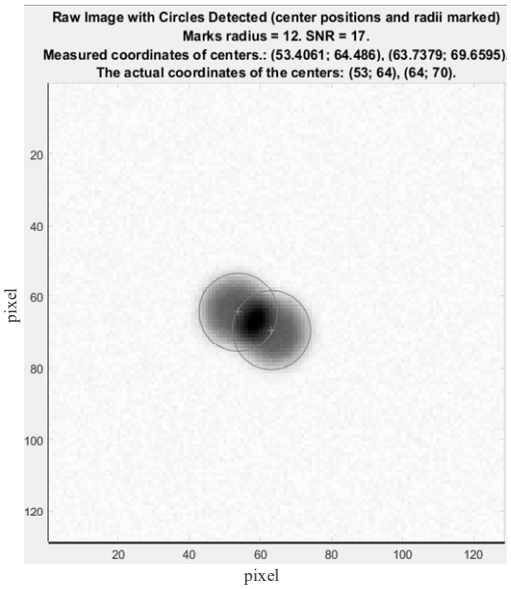

Fig.8 Indication of the measured centers of coordinates and the distance between the centers of the images

Step 2: The distance between the image centers is set as L, changing the step size from $2R$ to $6R$ with a step length of $0.1R$. There are no overlapping marks imagines in this process, so we use the weighted summation method to measure the center coordinates of the marked image[21], and the simulation result is shown in Fig.9 (the blue and purple lines).

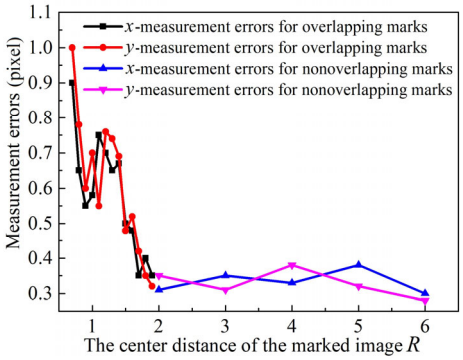

Fig.9 Measurement errors for overlapping marks and for nonoverlapping marks

Fig.9 shows the relationship between the measurement error of the image coordinate and the center distance of the marked image. The red line and blue line represent the measurement errors of the images moving along X-axis and Y-axis, respectively.

It can be seen from the simulation results, the supposed algorithm is unusable when the distance between the

centers of marks less than half the radius of the marks due to large measuring error. As the center distance of the marked image increases from 0.5*R* to 2*R*, the measurement error decreases gradually. For *L*=2*R*,…,6*R*, this value is equal to the average error of unoverlapping mark images. Therefore, the proposed collimator cannot be used within the radius *r*=0.5*R* of the image overlap area. Such as, when the radius of the receiver (CMOS) of the autocollimator is *R*′=12 pixel, and the size of each pixel is *p*=2.2 μm, the focal length of the objective lens is *f*=250 mm, the angle range that cannot be measured by the proposed autocollimator is:

$$\Theta_{\text{err}} = \frac{p \cdot 2 \cdot r}{2f} = \frac{p \cdot 2 \cdot 0.5 \cdot R}{2f}. \tag{13}$$

According to Eq.(13), Θ_{err}=11″, which is a small value compared with the measuring range of the autocollimator (15′).

Apart from, the analysis of the data determined that positioning accuracy is dependent only on the distance between the centers of the marks and the degree of the image overlapping. Parameters, such as the size of the matrix, the size of marks and other factors on the accuracy of coordinate measurement are not affected.

A prototype of the autocollimator based on the quadrangular pyramid was constructed and experiments were carried out to demonstrate the feasibility of the proposed method. The objective-lens focal length of the photoelectric autocollimator is 250 mm, the caliber and circle of confusion of which are 65 mm and 0.02 mm, respectively. The semiconductor diode "SFH 485P" with 10 mW power and 0.2 mm diaphragm diameter is employed as light source. The CMOS matrix "OV05620 CMOS QSXGA" with 2592×1944 resolution, 5.808 mm×4.294 mm sensitive area and 2.2 μm×2.2 μm pixel size is employed as the photoelectric sensor of the autocollimator. The 2D measurement range and measurement error of the autocollimator are 10′ and 1″, respectively, in case of conventional mirror reflector. The aperture diameter of the quadrangular pyramid is 50 mm. The experimental setup is shown in Fig.10. The quadrangular pyramid is mounted on the rotary stage. The distance from autocollimator to pyramid reflector is 900 mm. The calibrating mirror and calibrating autocollimator Triangle "Trioptics GMBH, Germany" are used to calibrate the angle measurements. The measurement range and accuracy of the calibrating autocollimator are 20′ and 1″, respectively.

The measurement experiment was conducted as follows:

Step 1: Firstly, the quadrangular pyramid was horizontally rotated for 15′ (Θ_1) by the calibrating autocollimator and rotation stage as the baseline of the measurement experiment. Secondly, the quadrangular pyramid was vertically rotated twenty times (Θ_2=Θ_i, *i*=1, 2, …, 21) in a step of 1′. Then the displacement of facula 2 in Fig.3 was measured by the calibrating autocollimator, corresponding to the displacement of the image spot after each rotation of the quadrangular pyramid.

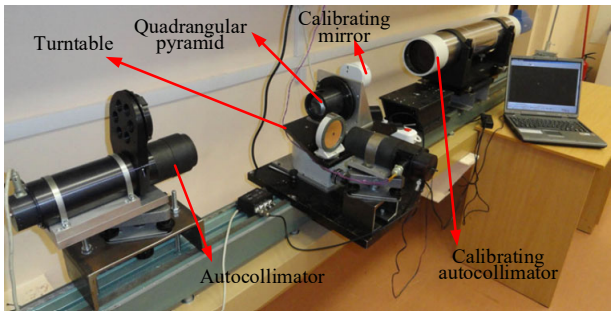

Fig.10 Photograph of the experimental setup

Step 2: The CMOS array of the autocollimator will take 10 frames, following by employing a weighted algorithm to determinstage 2 in Fig.3 was obtained. Finally, Θ_2 can be obtained according to Eq.(10), as depicted in Fig.9.

Step 3: Firstly, the quadrangular pyramid was horizontally rotated for 15′ (Θ_2) by the calibrating autocollimator and rotation stage as the baseline of the measurement experiment. Secondly, the quadrangular pyramid was vertically rotated twenty times (Θ_1=Θ_i, *i*=1, 2, ..., 21) in a step of 1′. Then the displacement of facula 1 in Fig.3 was measured by the calibrating autocollimator, corresponding to the displacement of the image spot after each rotation of the quadrangular pyramid.

Step 4: The CMOS array of the autocollimator will take 10 frames, following by employing a weighted algorithm to determine the central coordinates of the irradiance distribution of the image. By taking the mean of the central coordinate, the displacement of facula 1 in Fig.3 was obtained. Finally, Θ_1 can be obtained according to Eq.(10), as depicted in Fig.11.

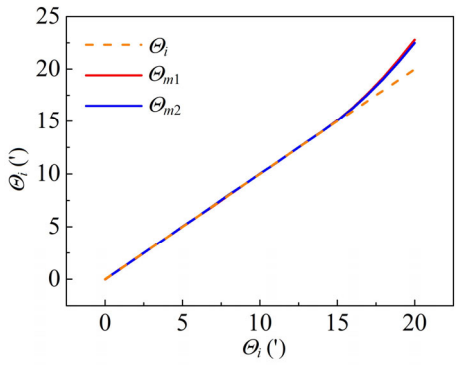

Fig.11 The measurements of the rotation angles Θ_1 and Θ_2, where the dash line depicts the linear fitting results of the measurement results

The results of Step 2 and Step 4 are shown in Fig.9.

According to the experimental results, the deviation between the measurement results of the rotation angle

and the linear fitting is derived random error of the autocollimator and the random error in the measurement range of 15′ was shown in Fig.12.

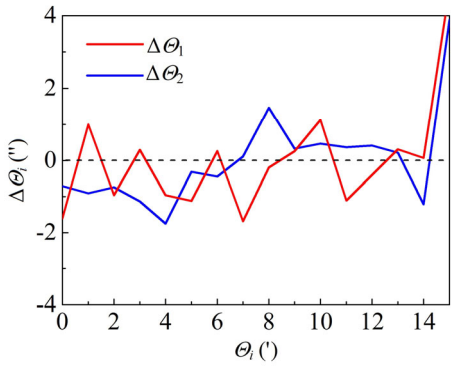

Fig.12 Random error of rotation angles Θ_1 and Θ_2 in a measurement range of 15′

It can be seen from Fig.10 that the root-mean-squares ($\Delta\Theta_1$ and $\Delta\Theta_2$) of the random error are 1.04″ and 1.4″, respectively. The estimation of the random error agrees well with the theoretical calculations. The measurement range of the autocollimator was improved from 10′ to 15′ by substituting the plane mirror with the proposed quadrangular pyramid.

In this paper, a photoelectric autocollimator based on the quadrangular pyramid is proposed to expanding the measurement range, and the corresponding algorithms are also deduced. To increasing the accuracy, a new image processing algorithm has been proposed, and the corresponding errors are also estimated. The research demonstrates that the error is less than a pixel, and the error does not exceed half a pixel when the distance between the marks more than two radii. Also, worth noting is the possibility of the algorithm to work with any number of marks and high noise immunity. The angle measurement experiments have been carried out to demonstrate the feasibility of the proposed method, and the experimental results have verified that the measurement range of the proposed quadrangular pyramid photoelectric autocollimator can be increased $\sqrt{2}$ times than that of the flat mirror photoelectric autocollimator from 10′ to 15′ arc minutes. The accuracy is better than 1″ when the deflection is less than 15′.

References

[1] T. Turgalieva and I. Konyakhin, Research of Autocollimating Angular Deformation Measurement System for Large-Size Objects Control, Proceedings of SPIE-The International Society for Optical Engineering **8788**, 878832 (2014).

[2] I. Konyakhin, T. V. Kopylova and A. I. Konyakhin, Optic-Electronic Autocollimation Sensor for Measurement of the Three-Axis Angular Deformation of Industry Objects, Proceedings of SPIE-The International Society for Optical Engineering **8439**, 84391N (2012).

[3] I. Konyakhin, T. V. Kopylova, A. I. Konyakhin and A. A. Smekhov, Proceedings of SPIE-The International Society for Optical Engineering **8759**, 87593E (2013).

[4] P. R. Yoder, E. R. Schlesinger and J. L. Chickvary, Applied optics **14**, 1890 (1975).

[5] M. Gao, Z. R. Dong, Z. L. Bian, Q. Ye, Z. J. Fang and R. H. Qu, Chinese Optics Letters **9**, 32 (2011).

[6] R. D. Geckeler, P. Křen, A. Just, M. Schumann, M. Krause, I. Lacey and V. V. Yashchuk, Review of Scientific Instruments **90**, 021705 (2019).

[7] R. P. Li, I. Konyakhin, Q. Zhang, W. Cui, D. D. Wen, X. H. Zou, J. Q. Guo and Y. Liu, Optical Engineering **58**, 104112 (2019).

[8] K. Ishikawa, T. Takamura, M. Xiao, S. Takahashi and K. Takamasu, Measurement Science & Technology **25**, 064008 (2014).

[9] J. Luo, Z. Wang, Z. Wen, M. Li, S. Liu and C. Shen, Review of Scientific Instruments **89**, 015101 (2018).

[10] W. Gao, H. Ohnuma, H. Satoh, H. Shimizu and S. Kiyono, CIRP Ann.-Manuf. Technol. **53**, 425 (2004).

[11] K. Ishikawa, T. Takamura, M. Xiao, S. Takahashi and K. Takamasu, Measurement Science & Technology **25**, 064008 (2014).

[12] S. J. Thompson, R. Lang, P. Rees and G. W. Roberts, Applied Optics **55**, 2827 (2016).

[13] Y. L Chen., Y. Shimizu, Y. Kudo, S. Ito and W. Gao, Optics Express, **24**, 15554 (2016).

[14] Y. L. Chen, Y. Shimizu, J. Tamada, Y. Kudo, S. Madokoro, K. Nakamura and W. Gao, Optics Express **25**, 16725 (2017).

[15] R. P. Li, M. Zhou, I. Konyakhin, K. Di and Y. Liu, Optics express **27**, 6389 (2019).

[16] I. A. Konyakhin, T. V. Turgalieva and R. P. Li, Proc. SPIE **9141**, 914123 (2014).

[17] Dennis F. Vanderwerf, Applied Prismatic and Reflective Optics, SPIE, Bellingham, Washington, 303 (2010).

[18] J. Lieblein, G. A. Korn and T. M. Korn, Mathematics of Computation **15**, 421 (2000).

[19] G. V. Pogarev and N. G. Kiselev, Optical Adjustment Problems: A Reference Book, Mashinostroenie, Leningrad, 206 (1989).

[20] D.H. Ballard, Pattern Recognition **13**, 111 (1981).

[21] A. F. Leandro, Pattern Recognition **41**, 299 (2008).

[22] Rafael C. Gonzalez, Richard E. Woods and Steven L. Eddins, Digital Image Processing Using Matlab **21**, 197 (2010).